PERGAMON

Pattern Recognition 32 (1999) 1463–1472

PATTERN RECOGNITION
THE JOURNAL OF THE PATTERN RECOGNITION SOCIETY

On the discrete representation of the Laplacian of Gaussian

Steve R. Gunn*

Image, Speech and Intelligent Systems Group, Department of Electronics and Computer Science, University of Southampton, SO17 1BJ, UK

Received 5 February 1998; received in revised form 3 November 1998; accepted 3 November 1998

Abstract

The Laplacian of Gaussian (LoG) is commonly employed as a second-order edge detector in image processing, and it is popular because of its attractive scaling properties. However, its application within a finite sampled domain is non-trivial due to its infinite extent. Heuristics are often employed to determine the required mask size and they may lead to poor edge detection and location. We derive an explicit relationship between the size of the LoG mask and the probability of edge detection error introduced by its approximation, providing a strong basis for its stable implementation. In addition, we demonstrate the need for bias correction, to correct the offset error introduced by truncation, and derive strict bounds on the scales that may be employed by consideration of the aliasing error introduced by sampling. To characterise edges, a zero-crossing detector is proposed which uses a bilinear surface to guarantee detection and closure of edges. These issues are confirmed by experimental results, which particularly emphasise the importance of bias correction. As such, we give a new basis for implementation of the LoG edge detector and show the advantages that such analysis can confer.

Keywords: Edge detection; Marr–Hildreth operator; Laplacian of Gaussian; Truncation effects; Edge detection error

1. Introduction

The Laplacian of Gaussian (LoG) has received much attention since it was proposed by Marr [1] as a physiological model of the early human visual system. Marr derived the LoG in trying to minimise spatial and bandwidth variance product of a filter in order to localise its influence. A different approach based on maximising the energy in the locality of the edge was developed by Shanmugam [2] and Lunscher [3], which produced a very similar function. The LoG is a multi-resolution operator that can be applied at different scales. This approach is common to many edge detectors [4,5] since the scale of interesting features is often unknown. The LoG has many desirable properties. The scaling of zero crossings [6,4] is such that edges consistently appear as scale space is traversed. It is also the only second-order differential operator that is both separable and rotation invariant [7]. Torre [8] has shown that the Gaussian is optimal for reducing noise with minimum delocalisation. However, it can suffer from response to phantom edges [9] and poor localisation around edges of high curvature [10,11], but methods have been developed for post-processing the edges [12,13] to attenuate these difficulties.

As Demigny [14] remarks, most optimal filters for edge detection are developed in the continuous domain and then transposed by sampling to the discrete domain. To implement the LoG in a practical image processing framework requires a finite sampled approximation. The

*Tel.: +44 1703 592338; Fax: +44 1703 594498; E-mail: S.R.Gunn@ecs.soton.ac.uk.

0031-3203/99/$20.00
PII: S0031-3203(98)00163-0

LoG can be implemented in both the spatial or frequency domain [15,16]. The infinite extent of the LoG in the spatial and frequency domain inhibits its direct use as an edge detector for finite sampled signals, and it is usually approximated by a truncated version which is optimal with respect to the MSE [17]. However, this truncation is generally achieved by a heuristic, such as a constant times the zero crossing of the LoG kernel. Incorrect choice of the constant will lead to poor edge detection and location [18,19]. In this paper, an analysis of the effects of truncation and sampling are considered to provide a firm basis for its discrete implementation.

To provide a rigorous bound on the mask size we propose a bound based on the fraction of energy ignored by the truncation. It is shown that consideration of this error provides a relationship between the edge detection error and the mask size employed. Truncating the LoG operator violates the zero mean property and it is shown how this can be compensated for by the introduction of a bias term. An analysis of the aliasing error introduced by sampling forms the basis for determining the appropriate range of scales over which the operator may be applied. In doing so it is shown that a commonly employed value of the scaling parameter, $\sigma = 1.0$, may be inappropriate depending on the level of adherence to the original description. In order to guarantee closure of the detected zero crossings, a scheme based on piece-wise bilinear interpolation is developed which by its continuity guarantees closure and a complete representation of the zero crossings, and hence the detected edges.

The paper takes the format: after reviewing the definition of the LoG, the effects of truncation are considered. Then the effects of sampling the LoG are developed. This is proceeded by a description of the zero-crossing detection employed. Finally, the theoretical results are compared with experimental results performed by applying various masks of different sizes and scales.

1.1. The laplacian of Gaussian

A two-dimensional Gaussian of standard deviation σ is given by

$$G(\mathbf{x}) = \frac{1}{2\pi\sigma^2} \mathrm{e}^{\|\mathbf{x}\|^2/2\sigma^2}, \tag{1}$$

where $\| \ \|$ is the Euclidean norm. The two-dimensional Laplacian is

$$\nabla^2 = \sum_{i=1}^{2} \frac{\partial^2}{\partial x_i^2}. \tag{2}$$

The Laplacian of Gaussian is given by

$$\nabla^2 G = \sum_{i=1}^{2} \frac{\partial^2 G}{\partial x_i^2} = G(\mathbf{x}) \sum_{i=1}^{2} \left(\frac{x_i^2}{\sigma^4} - \frac{1}{\sigma^2} \right)$$

$$= \frac{1}{2\pi\sigma^6} (\|\mathbf{x}\|^2 - 2\sigma^2) \mathrm{e}^{\|\mathbf{x}\|^2/2\sigma^2}, \tag{3}$$

and its Fourier transform is given by

$$F(\nabla^2 G) = -\|\xi\|^2 \mathrm{e}^{-\sigma^2\|\xi\|^2/2}. \tag{4}$$

The LoG is isotropic in the spatial and frequency domain, which is evident from Eqs. (3) and (4), and its cross-sections are plotted in Fig. 1. The frequency cross section, Fig. 1b, clearly illustrates its band pass characteristic. The peak magnitude response in the frequency domain is given by

$$\|\xi\| = \frac{\sqrt{2}}{\sigma}. \tag{5}$$

The crossing point in the spatial domain is given by

$$\|\mathbf{x}\| = \sigma\sqrt{2}. \tag{6}$$

Edges in Marr–Hildreth theory are determined by the zero crossings of an image convolved with the LoG operator. Although other second derivative based edge

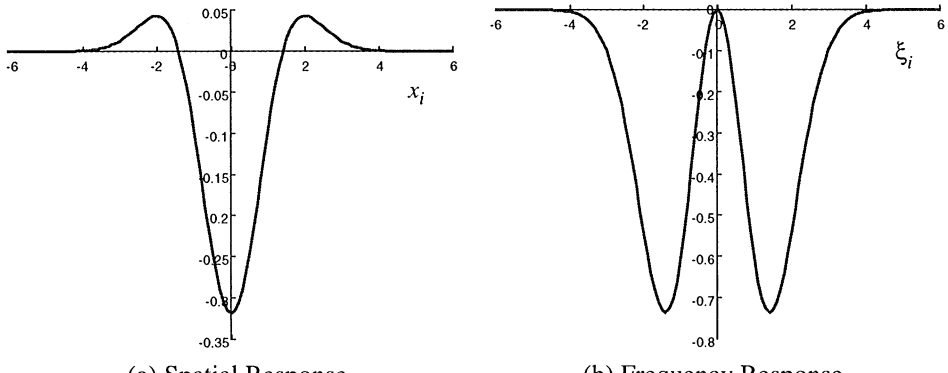

(a) Spatial Response (b) Frequency Response

Fig. 1. Spatial and frequency cross-section. ($\sigma = 1.0$)

detectors use the zero-crossing criteria for edge detection, the LoG is the only isotropic second derivative-based operator.

The LoG extends to infinity in both the spatial and the frequency domains and hence care must be taken in applying it in a finite domain. Should such care not be applied, the error introduced by truncation will significantly degrade the performance of the edge detector. In the next section, the consequences of truncation are considered. By considering the pixels of the image to be drawn from identical independently distributed Gaussians, it is shown that the probability of an error in edge detection can be expressed as a function of the truncation energy, and hence the mask size. This provides a strong basis for the determination of appropriate mask sizes based on the error probability.

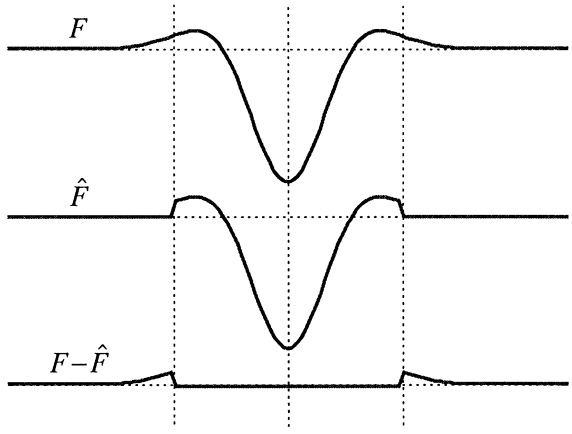

Fig. 2. Spatial domain truncation of the LoG (Axis Cross Section)

2. Truncation

The analysis of a truncated approximation to the LoG is divided as follows: In the first part, it is shown how the energy error (the fraction of energy lost due to truncation) is related to the mask size. Then it is demonstrated that a correction term must be added to the truncated operator to maintain an unbiased response to concave and convex edges. In the last part it is shown that the energy error of this truncated, bias corrected, operator is related to the probability of an error in zero-crossing detection and hence in the classification of edges.

2.1. Energy error

Fig. 2 illustrates the error, $F-\hat{F}$, introduced by approximating the LoG operator, F, with a truncated version, $\hat{F}$. It will be shown that the performance decreases monotonically with a decrease in truncation width, as would be expected. In application, the smallest possible truncation width is desirable for computational reasons.

In order to quantify this error, a rigorous scheme is developed from an analysis of the energy error, which is given by the fraction of energy lost from the signal due to truncation

$$\varepsilon = 1 - \frac{\int_{-l}^{l}\int_{-l}^{l} f(\mathbf{x})^2 \,\mathrm{d}x_1 \,\mathrm{d}x_2}{\int_{-\infty}^{\infty}\int_{-\infty}^{\infty} f(\mathbf{x})^2 \,\mathrm{d}x_1 \,\mathrm{d}x_2}, \tag{7}$$

where $f(x)$ is the spatial or frequency envelope for a finite square mask of size $2l \times 2l$. A square mask is chosen in preference to a radial mask since this is more suited to implementation within an image processing framework, although a similar analysis can be carried out for radial masks. Accordingly, the fraction of the energy that is ignored by restricting the LoG to the interval $(-l_s, l_s)$ in the spatial domain is given by

$$\varepsilon_s = 1 - \frac{\Gamma(\frac{5}{2}, l_s^2/\sigma^2)\,\Gamma(\frac{1}{2}, l_s^2/\sigma^2) + \Gamma(\frac{3}{2}, l_s^2/\sigma^2)^2 - 4\Gamma(\frac{3}{2}, l_s^2/\sigma^2)\,\Gamma(\frac{1}{2}, l_s^2/\sigma^2) + 2\Gamma(\frac{1}{2}, l_s^2/\sigma^2)^2}{\pi} \tag{8}$$

and by restricting the LoG to the interval $(-l_f, l_f)$ in the frequency domain by

$$\varepsilon_f = 1 - \frac{\Gamma(\frac{5}{2}, l_f^2\sigma^2)\,\Gamma(\frac{1}{2}, l_f^2\sigma^2) + \Gamma(\frac{3}{2}, l_f^2\sigma^2)^2}{\pi}, \tag{9}$$

where $\Gamma(\alpha, x)$ is the incomplete gamma function,

$$\Gamma(\alpha, x) = \int_0^x t^{\alpha-1}\mathrm{e}^{-t}\,\mathrm{d}t. \tag{10}$$

Letting $\mu_s = l_s/\sigma$ and $\mu_f = l_f\sigma$, be scale invariant parameterisations, the energy errors are shown in Fig. 3. The figures illustrate that the energy error decreases with increasing mask size. In the spatial domain the energy error decreases with decreasing σ and in the frequency domain the energy error decreases with increasing σ.

As μ becomes large, the energy errors in both the spatial and frequency domains converge, implying that the energy error decreases at the same rate. However, for smaller values of μ the graphs are different; the spatial domain energy error has an inflexion at $\mu_s = \sqrt{2}$ due to

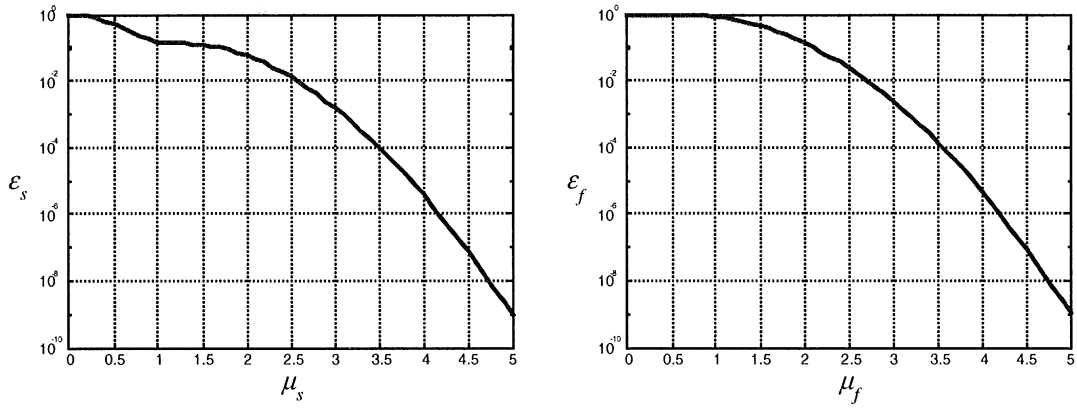

(a) Spatial Domain Energy Error (b) Frequency Domain Energy Error

Fig. 3. Energy Error Graphs

the zero crossing of the LoG operator in the spatial domain.

Choosing an appropriate level of energy error determines the mask sizes for implementation in the spatial or frequency domain. In the next section, it is shown how the truncation additionally introduces a bias, which must be compensated for to maintain the symmetry of the LoG operator to concave and convex edges.

2.2. Bias correction

The LoG operator has a zero mean, that is

$$\int_{-\infty}^{\infty}\int_{-\infty}^{\infty}\nabla^2 G(\mathbf{x})\,\mathrm{d}x_1\,\mathrm{d}x_2 = 0. \tag{11}$$

However, when the operator is truncated this property will be violated. Consequently, the edge detector will be biased towards concave or convex edges, since the response to a flat part of the image will be non-zero. To overcome this problem a bias correction, δ, must be added to the truncated operator, where

$$\delta = -\frac{1}{4l^2}\int_{-l}^{l}\int_{-l}^{l}\nabla^2 G(\mathbf{x})\,\mathrm{d}x_1\,\mathrm{d}x_2. \tag{12}$$

It is easily verified that the zero mean property is now restored

$$\int_{-l}^{l}\int_{-l}^{l}\nabla^2 G(x) + \delta\,\mathrm{d}x_1\,\mathrm{d}x_2 = 0. \tag{13}$$

The addition of this correction restores the zero mean property of Eq. (11). The operator has even been described incorrectly [20,21] where the zero mean condition is violated, due to an erroneous derivation of the operator.

2.3. Determination of zero-crossing detection error

In this section, the zero-crossing detection error that is introduced by application of a truncated mask in the spatial domain is related to the energy error introduced by truncation. If the LoG, F, is approximated by a bias corrected truncated version, $\hat{F}$, then the probability of an error is defined as the probability that the resulting convolutions of F and $\hat{F}$ with an image, I, differ in sign,

$$\begin{aligned} P_{error} &= P(F*I < 0 \wedge \hat{F}*I > 0) + P(F*I > 0 \wedge \hat{F}*I < 0) \\ &= P((F-\hat{F})*I < -\hat{F}*I \wedge \hat{F}*I > 0) \\ &\quad + P((F-\hat{F})*I > -\hat{F}*I \wedge \hat{F}*I < 0), \end{aligned} \tag{14}$$

where * denotes convolution. The residual distribution, $P_{F-\hat{F}}$, and the truncated distribution, $P_{\hat{F}}$, are independent and hence the error probability is given by,

$$\begin{aligned} P_{error} &= \int_{-\infty}^{0}\int_{0}^{-v} P_{\hat{F}}(u)\,P_{F-\hat{F}}(v)\,\mathrm{d}u\mathrm{d}v \\ &\quad + \int_{0}^{\infty}\int_{-v}^{0} P_{\hat{F}}(u)\,P_{F-\hat{F}}(v)\,\mathrm{d}u\,\mathrm{d}v \end{aligned} \tag{15}$$

A Gaussian distribution of mean, μ, and variance, σ, is given by

$$\mathrm{N}(\mu,\sigma) = \frac{1}{\sqrt{2\pi}\,\sigma}\,\mathrm{e}^{-(1/2)((x-\mu)/\sigma)^2}. \tag{16}$$

If the pixels are drawn from identical independent Gaussian distributions (we assume zero mean without loss of

generality), with variance σ_I, then the distribution of the pixel intensities is given by

$$P_I(x) = \mathrm{N}(0, \sigma_I). \tag{17}$$

The distribution of $\hat{F}$ is

$$P_{\hat{F}}(x) = \mathrm{N}(0, \sigma_{\hat{F}}\sigma_I), \tag{18}$$

where

$$\sigma_{\hat{F}}^2 = \int_{-l_s}^{l_s}\int_{-l_s}^{l_s} (\hat{F})^2 \,\mathrm{d}x_1\,\mathrm{d}x_2 \tag{19}$$

and the distribution of $F - \hat{F}$ is

$$P_{\hat{F}}(x) = \mathrm{N}(0, \sigma_{F-\hat{F}}\sigma_I), \tag{20}$$

where

$$\sigma_{F-\hat{F}}^2 = \int_{-\infty}^{\infty}\int_{-\infty}^{\infty} (F - \hat{F})^2 \,\mathrm{d}x_1\,\mathrm{d}x_2. \tag{21}$$

Hence from Eqs. (15), (18) and (20) the error is given by

$$P_{error} = \frac{1}{\pi}\tan^{-1}\left(\frac{\sigma_{F-\hat{F}}}{\sigma_{\hat{F}}}\right). \tag{22}$$

Considering the truncation error from Eq. (7) the fraction of energy ignored by truncation can be expressed as

$$\varepsilon = 1 - \frac{\sigma_{\hat{F}}^2 + 4l_s^2\delta^2}{\sigma_F^2 + \sigma_{F-\hat{F}}^2}. \tag{23}$$

From the Cauchy Schwarz inequality,

$$\int_{-l_s}^{l_s}\int_{-l_s}^{l_s} (F)^2 \,\mathrm{d}x_1\,\mathrm{d}x_2 \geqslant \left(\int_{-l_s}^{l_s}\int_{-l_s}^{l_s} F \,\mathrm{d}x_1\,\mathrm{d}x_2\right)^2,$$

$$\sigma_{\hat{F}}^2 + 4l_s^2\delta^2 \geqslant 16l_s^4\delta^2 \tag{24}$$

$$\sigma_{\hat{F}}^2 \geqslant 4l_s^2\delta^2(4l_s^2 - 1).$$

Hence, if $l_s^2 \gg \frac{1}{2}$ then,

$$\sigma_{\hat{F}}^2 \gg 4l_s^2\delta^2 \tag{25}$$

and therefore,

$$\varepsilon \approx 1 - \frac{\sigma_{\hat{F}}^2}{\sigma_{\hat{F}}^2 + \sigma_{F-\hat{F}}^2} \Rightarrow \frac{\sigma_{F-\hat{F}}}{\sigma_{\hat{F}}} \approx \sqrt{\frac{\varepsilon}{1-\varepsilon}}. \tag{26}$$

It follows from Eqs. (22) and (26) that the probability of an incorrect edge classification is given by

$$P_{error} \approx \frac{1}{\pi}\sin^{-1}(\sqrt{\varepsilon}), \tag{27}$$

or alternatively the energy error is given by

$$\varepsilon \approx \sin^2(\pi P_{error}). \tag{28}$$

As such the likelihood of error is intimately related to the truncation of the operator, reducing the truncation error reduces the likelihood that false zero crossings will be detected or true zero crossings will be ignored.

2.4. Summary

The following strategy may be employed to ascertain a suitable mask size for spatial domain implementation of the LoG. Choosing the probability of an edge detection error determines the fraction of energy ignored by truncation from Eq. (28). Hence, from Fig. 3a, or numerical inversion of Eq. (8) it is possible to determine the required mask sizes to attain the required error performance.

3. Discrete formulation

The discussion so far has been concerned with the truncation of a continuous LoG operator. However, for implementation on a digital computer the continuous operator must be approximated by a discrete mask. The elements of the mask are obtained by sampling the continuous LoG on a discrete grid. In the following discussion it is assumed that the mask elements are stored in double-precision floating point format.

3.1. Determination of mask sizes and scales

The discrete mask widths w_s, w_f in the spatial and frequency domain, respectively, are given by

$$w_s = 1 + 2\lceil l_s \rceil = 1 + 2\lceil \mu_s\sigma \rceil,$$

$$w_f = 1 + 2\left\lceil l_f\frac{N}{2\pi}\right\rceil = 1 + 2\left\lceil \frac{\mu_f N}{\sigma\, 2\pi}\right\rceil, \tag{29}$$

where $\lceil x \rceil$ rounds up to the nearest integer.

3.2. Aliasing error and bounds on the scale parameter

The values of the scale parameter, σ, that are appropriate are restricted by the discrete representation. As σ becomes smaller the lobes of the LoG operator are pulled closer and closer together in the spatial domain, and eventually the operator will become too compact to be described accurately with a unitary sampling interval. Accordingly, in the frequency domain as σ decreases the width of the band-pass filter expands until it is larger than the frequency representation. This corresponds to a scale that is below the sampling width of the discrete representation. Consider an image of size $N \times N$ with unit sampling interval in the spatial domain. If no extra aliasing is introduced then the minimum value of sigma is given by

$$w_f < N \Rightarrow \sigma > \frac{\mu_f}{\pi}\frac{N}{N-2}. \tag{30}$$

Similarly, the maximum size is constrained by the spatial representation of the function, which must be less than or equal to the spatial signal size. (Note that since the signal is being convolved typically it will have to be significantly less than the signal size.) Hence, the maximum value of sigma is given by

$$w_s < N \Rightarrow \sigma < \frac{N-3}{2\mu_s} \tag{31}$$

Combining Eqs. (30) and (31) gives the following bounds on σ:

$$\frac{\mu_f \quad N}{\pi N - 2} < \sigma < \frac{N-3}{2\mu_s}. \tag{32}$$

To illustrate how the mask sizes and scales can be determined, consider the following example. Let an acceptable zero-crossing detection error be 0.1%, then $\varepsilon_s \approx 9.9 \times 10^{-6}$ from Eq. (28). From Fig. 3a this corresponds to a scale invariant mask width of $\mu_s \approx 3.8$. Choosing the truncation error $\varepsilon_s = \varepsilon_f$ determines $\mu_f \approx 3.8$ from Fig. 2b. Hence from Eq. (32), appropriate bounds on σ for a 256×256 image are,

$$1.22 < \sigma < 33.3. \tag{33}$$

and the mask sizes are given by

$$w_s = 1 + 2\lceil 3.8\sigma \rceil, \quad w_f = 1 + 2\left\lceil \frac{154.8}{\sigma} \right\rceil \tag{34}$$

which are shown in Fig. 4.

A commonly employed heuristic for determination of the mask size is three times the distance between the zero crossings in the spatial domain [22] ($\approx 8.5\sigma$). This is comparable to w_s from Eq. (34), and hence implies a zero-crossing detection error of approximately 0.1%.

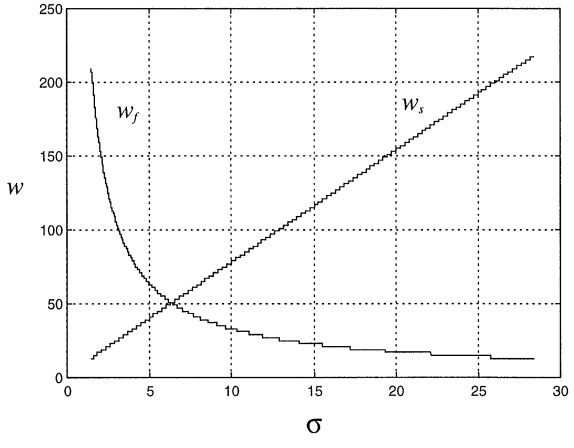

Fig. 4. Mask size vs. scale for 0.1% zero crossing detection error (256×256 image)

3.3. Bias correction

The bias introduced by the discrete mask is removed by adding a correction term, δ_d, to restore the zero mean property (Eq. (11)),

$$\delta_d = -\frac{1}{w_s^2} \sum_{x_1 = -((w_s-1)/2)}^{((w_s-1)/2)} \sum_{x_2 = -((w_s-1)/2)}^{((w_s-1)/2)} \nabla^2 G(\mathbf{x}). \tag{35}$$

An alternative approach for guaranteeing the zero mean property for the discrete mask has been used [18, 20,21]. However, this method distorts the shape of the LoG in order to ensure the elements sum to zero, and as such is not an accurate representation of the LoG.

3.4. Summary

To implement the LoG for $N \times N$ images a square discrete mask can be used. Given an acceptable error performance for the edge detection, the truncation error can be determined from Eq. (28). This determines the mask size from Eq. (8) up to the scale parameter. The required scale, σ, must satisfy the bounds of Eq. (32), before the mask can be employed. Finally, a bias correction is introduced to ensure that all the elements sum to zero. The operation may be performed by convolution in the spatial domain or by multiplication in the frequency domain. To complete the edge detection scheme, the edges are determined by the zero crossings of the resultant signal. In the next section a simple, but consistent zero-crossing detector is described.

4. Zero-crossing detection

There is a scarcity of literature on the zero-crossing detection required in the edge classification stage. To address this, a method based on a piece-wise bilinear interpolation of the resulting LoG convolved signal is proposed. The important characteristic of this representation is that it is continuous, guaranteeing complete zero-crossing detection, and hence closure of the zero-crossing contours. The method gives a zero-crossing resolution equal to that of the image. Alternatively, a sub-pixel technique such as that of Huertas [22] or Nalwa [23] can be employed to increase the resolution of the zero crossings, at the cost of extra computation. The scheme is illustrated for the 1-D case in Fig. 5. A zero crossing will exist if the interpolation crosses the axis in the interval $[x - \frac{1}{2}, x + \frac{1}{2})$. The half open interval is used to ensure that a zero crossing occurring on the boundary will only be classified once.

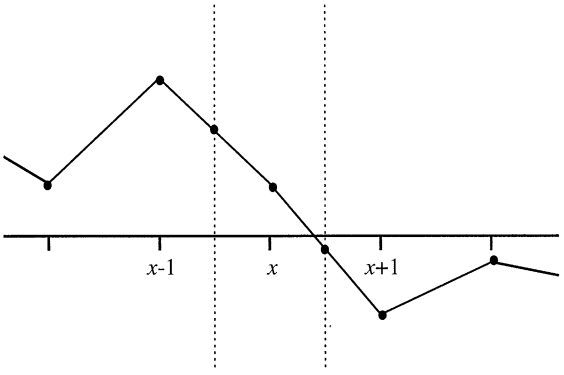

Fig. 5. Zero Crossing Detection.

Accordingly, a zero crossing can be detected by determining the signs of the three points $f(x-\frac{1}{2})$, $f(x), f(x+\frac{1}{2})$. Extension to the two-dimensional case is achieved as follows. Let Ω be a matrix,

$$\Omega = \begin{bmatrix} f_{x-\frac{1}{2},y+\frac{1}{2}} & f_{x,y+\frac{1}{2}} & f_{x+\frac{1}{2},y+\frac{1}{2}} \\ f_{x-\frac{1}{2},y} & f_{x,y} & f_{x+\frac{1}{2},y} \\ f_{x-\frac{1}{2},y-\frac{1}{2}} & f_{x,y-\frac{1}{2}} & f_{x+\frac{1}{2},y-\frac{1}{2}} \end{bmatrix} \tag{36}$$

with indices $[-1,0,1]\times[-1,0,1]$, and whose elements can be determined by convolution of the LoG convolved image with various 3×3 masks. A zero crossing will exist in the region $[x-\frac{1}{2}, x+\frac{1}{2})\times[y-\frac{1}{2}, y+\frac{1}{2})$ if

$$((\exists_{i,j}:\Omega_{i,j}>0)\wedge(\exists_{i,j}:\Omega_{i,j}<0))$$
$$\vee((\exists_{i,j}:(\Omega_{i,j}=0\wedge(i+2j>0)))\wedge(\Omega_{0,0}\neq 0), \tag{37}$$

where $i,j\in\{-1,0,1\}$. The first term defines a zero crossing if there are positive and negative values in the neighbourhood of the pixel. The second term considers the additional case where the zero crossing occurs at the boundary. This expression can be implemented efficiently as a lookup table, with 3^9 values.

5. Experimental determination of LoG performance

To compare the theoretical performance with experimental results, investigations were carried out with various test images. An obvious choice is the Lenna image [24], (Fig. 5a). A performance measure,

$$ZC_{error} = \frac{\text{Number of false zero crossings} + \text{Number of missed zero crossings}}{\text{Number of pixels}} \tag{38}$$

based on the correct classification of zero-crossings of the LoG was chosen for evaluation. This was chosen because it provides a comparable measure to that of the probability of edge detection error, P_{error}, enabling a comparison of the experimental results with the theory of Section 2.

The experimental tests employed a discrete square mask with double precision elements, and the zero-crossing detector described in the previous section. An example of the edge contours obtained from the LoG

(a) Original Image (512×512, 8bits/pixel)

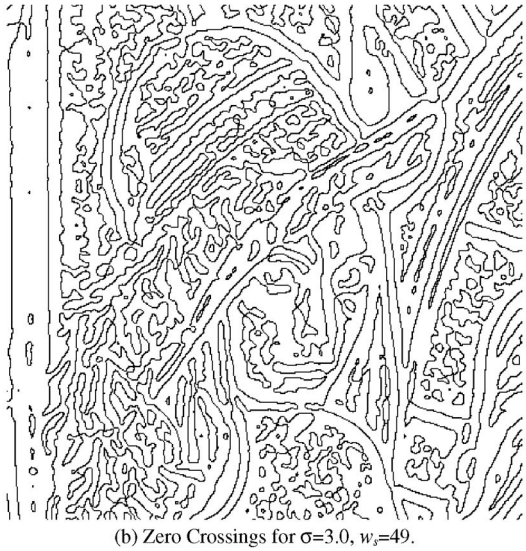

(b) Zero Crossings for σ=3.0, w_s=49.

Fig. 6. Lenna Image.

operator is illustrated in Fig. 6b, and it is evident that the zero crossing detector retains the continuity properties of the extracted edges. To test the performance of the LoG implementation, the value of ZC_{error} was measured for three different scales ($\sigma = 1.0$, 2.0 and 3.0), and for odd mask sizes in the range $w_s = 3, \ldots, 31$. A mask size of $w_s = 49$ was used as a reference to compute the ZC_{error}. The performance degradation as the mask size is reduced is illustrated in Fig. 7 for the bias corrected masks. Fig. 7a shows the ZC_{error} against the mask width demonstrating that larger scales require larger masks, and that the performance of the edge detector increases with increasing mask size. Fig. 7b shows the ZC_{error} re-plotted against the scale normalised mask width, along with the predicted error P_{error}. It is evident that the experiments agree well with theory for large values of μ_s. It is also clear from Fig. 7b that the $\sigma = 1.0$ curve provides slightly better performance when compared with higher scales. However, strictly $\sigma = 1.0$ lies outside the bounds of Eq. (32) and hence there may be some error in the reference zero-crossings image used. It was used in the experiments since it is a commonly quoted value for the scale parameter in the LoG operator.

To illustrate the importance of the bias correction the experiments were repeated without this correction. The results are shown in Fig. 8. It is clear that the performance is degraded with respect to Fig. 7. Most notably the improvement in performance is negligible until $\mu_s > 3$, when the performance starts to increase. However, in the range of interest, $\mu_s > 3$, the bias corrected version Fig. 7b always outperformed the uncorrected version, (Fig. 8b).

The importance of the bias correction is further illustrated in Fig. 9, which shows the zero-crossing detection errors for a mask with bias correction (Fig. 9a), and a mask without bias correction, (Fig. 9b). The

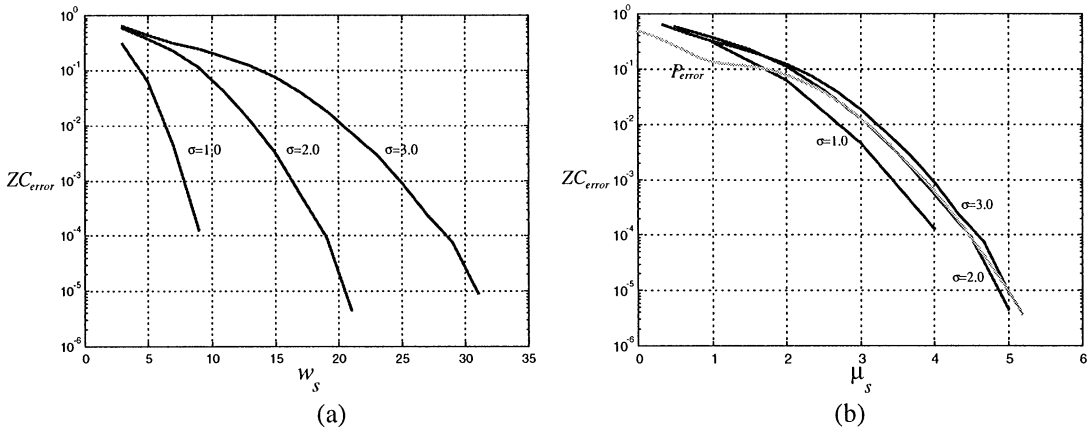

Fig. 7. Zero Crossing Detection Error for bias corrected mask.

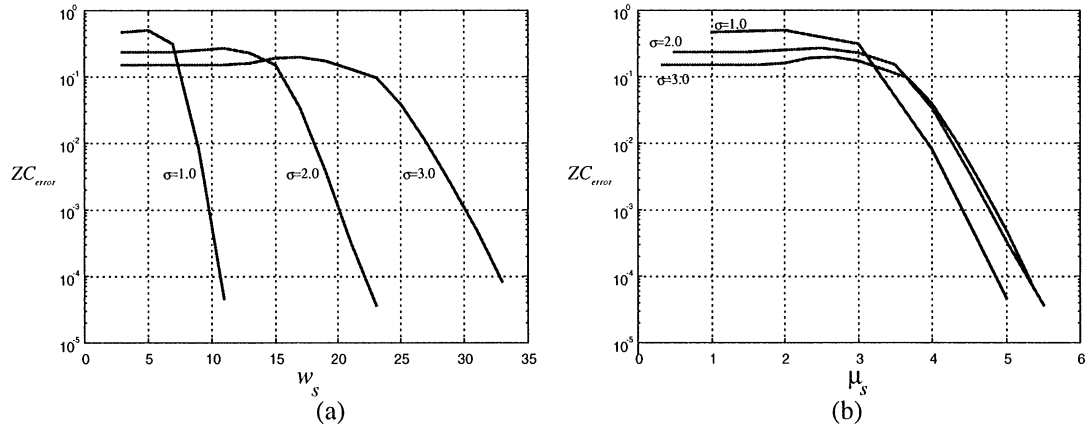

Fig. 8. Zero Crossing Detection Error for non-bias corrected mask.

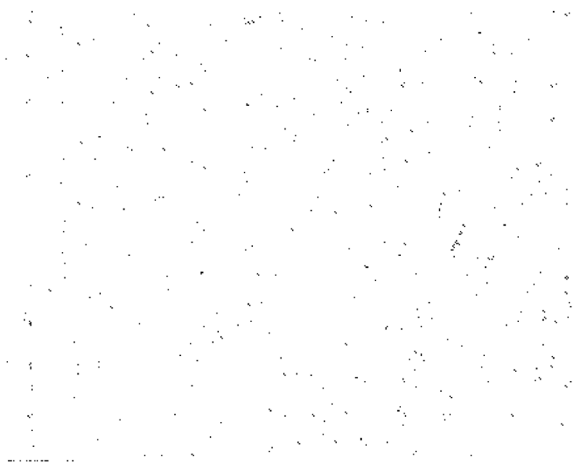

(a) with bias correction

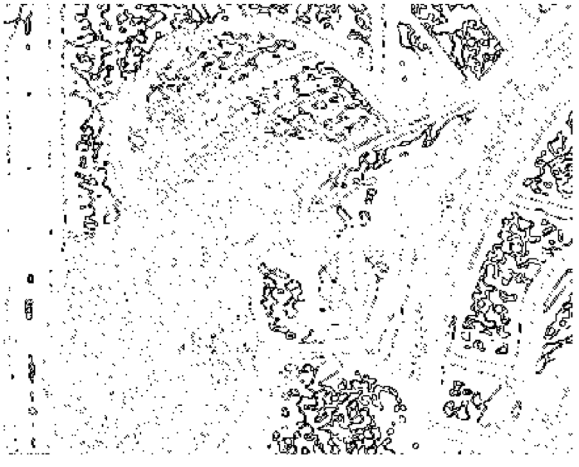

(b) without bias correction

Fig. 9. Zero Crossing Errors for $\sigma = 3.0$, $w_s = 23$.

degradation in performance for the bias corrected mask is small and spatially uncorrelated, whereas the degradation when no bias correction is used is significant and spatially correlated.

6. Conclusions

The LoG operator is a commonly used edge detector, but its discrete implementation is often applied heuristically. In this paper, we have shown that the zero-crossing detection error can be related to the mask size used, by consideration of the fractional energy error introduced by truncation. Experimental results have been shown to confirm the predicted errors. This provides a solid basis for determining appropriate mask sizes. By consideration of the aliasing error in both the frequency domain and the spatial domain it has been shown that there are bounds on the range of acceptable values for the scale parameter. Additionally, the importance of a bias correction has been demonstrated. A discrete zero-crossing detector has been developed that guarantees closure of the extracted contours and hence is consistent with the Marr–Hildreth theory of edge detection. Together, these results provide a basis for the robust implementation of the LoG operator.

References

[1] D. Marr, E. Hildreth, Theory of edge detection, Proc. Roy Soc. Lond. B 207 (1980) 187–217.

[2] K. S. Shanmugam, F.M. Dickey, J.A. Green, An optimal frequency domain filter for edge detection in digital pictures, IEEE Trans. Pattern Anal. Mach. Intell. 1 (1) (1979) 37–49.

[3] W.H.H.J. Lunscher, The asymptotic optimal frequency domain filter for edge detection. IEEE Trans. Pattern Anal. and Mach. Intell. 5 (6) (1983) 678–680.

[4] A.P. Witkin, Scale-space filtering, Int. Joint Conf. of Artificial Intelligence, Morgan Kaufmann Publishers, Inc., San Mateo, CA, 1983, pp. 1019–1022.

[5] L.M. Kennedy, M. Basu, Image enhancement using a human visual system model, Pattern Recognition 30 (12) (1997) 2001–2014.

[6] A.L. Yuille, T. A. Poggio, Scaling theorems for zero crossings, IEEE Trans. Pattern Anal. Mach. Intell. 8 (1) (1986) 15–25.

[7] V. Lacroix, Edge detection: what about rotation invariance? Pattern Recognition Lett. 11 (1990) 797–802.

[8] V. Torre, T.A. Poggio, On edge detection, IEEE Trans. Pattern Anal. Mach. Intell. 8 (2) (1986) 147–163.

[9] L. Alparone, S. Baronti, A. Casini, A novel approach to the suppression of false contours originated from Laplacian-of Gaussian zero-crossings, Proc. IEEE Int. Conf. on Image Processing ICIP96, vol. 3, 1996, pp. 825–828.

[10] F. Ulupinar, G. Medioni, Refining edges detected by a LoG operator, Comput. Vision Graphics Image Process. 51 (1990) 275–298.

[11] J. Koplowitz, V. Greco, On the edge location error for local maximum and zero-crossing detectors. IEEE Trans. Pattern Anal. Mach. Intell. 16 (12) (1994) 1207–1212.

[12] J.S. Chen, G. Medioni, Detection, localization, and estimation of edges, IEEE Trans. Pattern Anal. Mach. Intell. 11 (2) (1989) 191–198.

[13] J.J. Clark, Authenticating edges by zero-crossing algorithms, IEEE Trans. Pattern Analy. Mach. Intell. 11 (1) (1989) 43–57.

[14] D. Demigny, T. Kamlé, A discrete expression of Canny's criteria for step edge detector performance evaluation, IEEE Trans. Pattern Analy. Mach. Intell. 19 (11) (1997) 1199–1211.

[15] G. Cortelazzo, D.D. Giustina, G.A. Mian, Frequency domain design of FIR and IIR Laplacian of Gaussian filters for edge detection, Circuits Systems Signal Process. 15 (5) (1996) 555–572.

[16] M.R.B. Forshaw, Speeding up the Marr-Hildreth operator, Comput. Vision Graphics Image Process. 41 (1988) 172–185.
[17] L.J. van Vliet, I.T. Young, A nonlinear Laplace operator as edge detector in noisy images, Comput. Vision Graphics Image Process. 45 (1989) 167–195.
[18] R.M. Haralick, Digital step edges from zero crossing of second directional derivatives, IEEE Trans. Pattern Anal. Mach. Intell. 6 (1) (1984) 58–68.
[19] W.E.L. Grimson, E.C. Hildreth, Comments on "Digital step edges from zero crossings of second directional derivatives", IEEE Trans. Pattern Analy. Mach. Intell. 7 (1) (1985) 121–127.
[20] A.K. Jain, Fundamentals of Digital Image Processing, Prentice-Hall, Englewood Cliffs, NJ, 1989.
[21] M. Sonka, V. Hlavac, R. Boyle, Image Processing, Analysis and Machine Vision, Chapman & Hall London, 1993.
[22] A. Huertas, G. Medioni, Detection of intensity changes with subpixel accuracy using Laplacian–Gaussian masks. IEEE Trans. Pattern Analy. Mach. Intell. 8 (5) (1986) 651–664.
[23] V.S. Nalwa, Edge detector resolution improvement by image interpolation, IEEE Trans. Pattern Analy. Mach. Intell. 9 (3) (1987) 446–451.
[24] The Rest of the Lenna Story. Available at ⟨http://www.cs.cmu.edu/~chuck/lennapg/lenna.shtml⟩

About the Author—STEVE GUNN received his BEng. and Ph.D. (1996) from the University of Southampton. He is currently a Lecturer in Intelligent Systems at the University of Southampton. His research interests include computer vision, active contours, support vector machines and neural networks.